Property mapping of LDPE during 3D printing: Evaluating morphological development with X-ray Scattering

Daniel P. da Silva[1], João Pinheiro[1], Saba Abdulghani[1], Christina Kamma-Lorger[2], Juan Carlos Martínez[2], Eduardo Solano[2], Artur Mateus[1], Paula Pascoal-Faria[1] and Geoffrey R. Mitchell[1]*

[1]Centre for Rapid and Sustainable Product Development, Polytechnic Institute of Leiria, Marinha Grande, Portugal

[2]NCD-SWEET beamline, Alba Synchrotron Light Source, Cerdanyola del Vallès, Barcelona, Spain

*** Correspondence:**
Geoffrey R. Mitchell
geoffrey.mitchell@ipleiria.pt

Keywords: Direct digital manufacturing; 3D printing, extrusion, fused granular fabrication, LDPE, polymer morphology, crystallization, SAXS/WAXS.

Abstract

As part of the industry 4.0 implemented solutions, direct digital manufacturing has been addressed as one of the key tools and it enables creation of products directly through digital definition. Commonly known as additive manufacturing, it comprises a set of technologies that are expressively agile in small-scale productions and prototyping and, in comparison to conventional mass manufacturing processes, such as injection molding of plastics. It streamlines mass customization and allows the production of highly complex objects; promoting new shapes obtained by generative design, weight reduction, and the concept of virtual part stocks for maintenance and production inventory.

It has been broadly applied in several fields, from medical devices to the aerospace industry. A new era of design possibilities and accessibility was unveiled; however, most developments are focused, merely, on shape reproduction precision and the development of new feeding systems and materials. This work is focused on a shift in design for additive manufacturing, where the defined polymer properties, by means of the adjustment of the process conditions, constitute a decision-making variable. In order to evaluate the morphology of semicrystalline polymers during extrusion-based 3D printing, in-situ time-resolving small and wide-angle X-ray scattering measurements were performed at the ALBA synchrotron light source in Barcelona. The ultimate goal of this research is to develop a material property mapping methodology during semicrystalline polymer melt extrusion-based 3D printing. For this purpose, some printing trials were performed with low-density polyethylene, and it was possible to observe a correlation between the extrusion rate, writing speed, and the level of anisotropy induced by the manufacturing parameters.

1 Introduction

Direct Digital Manufacturing (DDM) consists of a decentralized scheme of manufacturing where designers and individuals (as consumers and makers) conceptualize products and innovative solutions allowing them to obtain small batches and mass customization for end users, making use of additive manufacturing as a base of the spectrum of technical solutions in which is possible to obtain

final parts and prototypes directly from a computer-aided design (CAD) file within a digital network and, optionally, validated through computer-aided engineering (CAE) software (1–3).

In comparison to conventional manufacturing technologies, DDM has enabled a more agile exploration of complex designs, and prototyping has become much faster and less expensive. Moreover, it has been established in industrial and commercial low-volume productions, and for customized tools (e.g., jigs, fixtures) (2). It is assumed that scientists and engineers have another set of technical solutions when designing for manufacturing, especially while working on complex and optimized geometries, engineered with topology optimization, generative design, or, simply, different infill strategies.

The advantage of mass customization is also beneficial for biomedical applications, where doctors and engineers combine strategies to create custom-fitting products for patients, such as in regenerative medicine, cancer therapies, and drug delivery systems (4).

Additive manufacturing (AM) comprises a variety of materials and processes, with extrusion-based technologies (such as FDMTM /FFF - fused deposition modeling TM/ fused filament fabrication) being the most accessible and popular solutions. Usually fed with filaments containing thermoplastic polymers, FDMTM/FFF equipment heat the material above the melting point, extrude it, and deposit it layer by layer, in predetermined patterns onto a build platform and predecessor layers, in order to complete a certain geometry (5,6).

In the last few years, many advances in 3D printing have been achieved, such as: object shape reproduction with higher accuracy (geometric and dimensional); higher print speeds (7); feeding systems along with material selection; and component integration (8). The range of available materials has followed this trend, widening to respond to the functionality requirements of the manufactured parts, including fiber reinforcement (9).

Attention has been given to the process parameters, such as printing temperatures and velocities, in order to optimize polymer melt flow rate (10). Besides that, there is an awareness of the influence of the manufacturing variables on the mechanical properties of the printed parts, as with any polymer processing technology (6). In some cases, in situ X-ray scattering analysis was performed along the printed layers, comparing the crystallization at different heights of the deposited strands, but lacking the evaluation along the write (print) direction with the variation of the fundamental processing parameters (11,12). In a similar way, but with the combined assessment of the temperature profile of the print, this technique was also used to infer the influence of the temperature profile on the degree of crystallinity (13). However, there is not a focus on the material design itself, beyond the domain of geometry replication.

The aim of this work is to address this area, introducing a new stage of design for additive manufacturing (DfAM). Ideally, the material properties can be mapped on de-mand along an entire part, through the control of the process parameters.

The challenge consists of understanding the correlation between the control inputs and the physical properties of the parts. This is the focus of this work, in which fused granular fabrication was used to perform printing trials with distinct sets of parameters, while analyzing the morphology development of the polymer melt; and in line with the previously reported work (14,15).

1.1 Fused Granular Fabrication

Fused granular fabrication (FGF) (or fused particle fabrication) (10) is an extrusion-based process that uses plastic pellets instead of a filament as the feedstock. In practice, it is a suitable approach for the production of bigger parts, and for the exploitation of the materials available on the market (typically deployed in injection molding) or custom compo-sites.

Usually, virgin material is obtained in pellet shape, and the same happens with recycled materials. Obtaining filament rolls implies an additional step, where the material is extruded with a certain diameter (usually 1.75mm or 3mm) and then wound. This filament production process might result in a slight degradation of the material, which can be considered a disadvantage of filament-fed 3D printers (16,17). Besides, the use of pellets is very straightforward, and associated extrusion systems permit a relatively constant extrusion rate (with an even flow of homogeneous melt and without material feed blockages).

This work is based on a pellet-fed production, and, despite the availability of a large number of materials, and their grades, in this shape for injection molding, as an example; the successful implementation in 3D printing with melt deposition is deeply compromised by an elaborated set of distinct parameters and conditions, in comparison to conventional production technologies. In other words, the availability of a wider range of materials does not immediately mean that the pellet-shaped raw matter can be suitable for 3D printing. Instead, it means their potential applicability can be studied and explored. The FGF 3D printers share the same platforms FDM™/FFF printers, the only difference re-lies on the feeding/extruder system. Instead of a filament intake mechanism for the material to be pushed through a hot end, the extruder has a pellet hopper or a melt reservoir, to store and furtherly introduce the material in a solid or liquid state respectively, in the extruder barrel with a rotating extrusion screw (18–20). An alternative approach consists of filling a chamber with granules and utilizing a piston to press the heated material (21). The representation of these configurations can be observed in Figure 1.

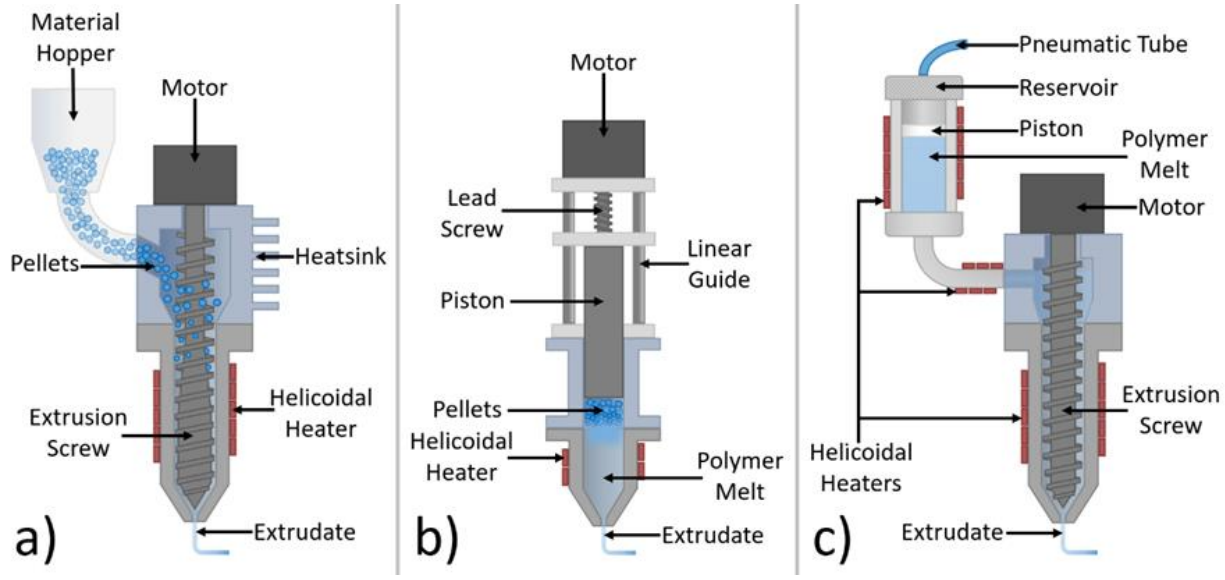

Figure 1 - Representation of the types of fused granular fabrication extruders. a) extruder chamber directly fed with pellets; b) pellets placed and melt in the piston/plunger chamber; c) pellets placed and melt in the reservoir.

Basically, material feeding can occur in two ways: directly loading the extruder with pellets or loading it with the polymer melt.

In configuration a), from the reservoir, the beads enter the extrusion chamber (by gravity, or compressed air, and the motion of the screw itself), which has to be cooled to allow the transportation, at the feed zone, of the plastic material to the heated part where it is compressed and melt.

Configuration b) requires a full retraction of the piston to allow the refill of the chamber, the pellets are then compressed and melted in the same extruder part.

With configuration c), the material is placed and heated in a separate reservoir. The transport of the polymer melt is done by means of the movement of a piston, loaded with compressed air. Notice

that this configuration has three main heating zones: feeder, channel, and extruder body. Therefore, despite guaranteeing a uniform flow rate of material, this adds variables to control, to a list of parameters commonly involved in this form of additive manufacturing.

- Feeding system
  - Gravity
  - Size of the beads
  - Air pressure
  - Chamber heating
  - Polymer rheology
- Extruder temperature
  - Heating power
  - Insulation
  - Thermal conductivity and Heat dissipation of the extruder's body
  - Cooling system
- Extrusion rate/speed
  - Feeding system
  - Power input and mechanical transmission
  - Compression ratio
- Write/Print speed
  - Power input and mechanical transmission
  - Vibrations and damping
  - Mechanical elements and movement precision
  - Write/print and extrusion speed function (22)
  - Adhesion to bed/platform or to the previously deposited layers of material
- Printing platform/bed
  - Levelling
  - Platform material and finishing (for adhesion and/or heat conduction)
  - Bed temperature
- Nozzle/hot end configuration
  - Diameter
  - Length
    - Length-to-diameter ratio
  - Temperature
  - Material of the nozzle body
  - Geometry of the nozzle body
- Material
  - Rheology
    - Viscosity and melt flow index (MFI)
    - Temperature
    - Pressure
  - Thermal conductivity of the extrudate
  - Temperature differential between the layers
- Cooling system
  - Extrusion temperature

    - Thermal conductivity of the extrudate
    - Temperature of bed/platform or previously deposited layers of material
- Surrounding environment
    - Enclosure hermeticity
    - Ambient temperature (air and radiant temperatures in closed and open environments)
    - Heat and matter transfer (air draughts and convection influence)
    - Humidity

Exploring materials limits in 3D printing requires a set of instruments in order to monitor, control, and contour the above-listed variables (the levels of the list express the dependencies of each main parameter).

The time response of the input parameters differs between them, and for an "on de-mand" and "on the fly" control, it is rather convenient to have a practically instantaneous transition of the real value to the successive setpoints. Beyond that, the property mapping depends on the time it takes for the parameter shifts to have an effect on the material morphology, and the amount of time for relaxation and/or crystallization. The importance of these factors lies in the resultant precision and resolution of the induced property texture into the object's material.

In practice, when set and read from the g-code file, a shift in extrusion rate or print speed happens substantially quicker than with the extrusion temperature. Not only this last variable has a noticeable delay associated, but it also has a more unstable behavior with successive heating and cooling switches around the target value, within a certain interval (overshooting and undershooting).

Although an effective extrusion temperature control could be employed, this paper focuses on the changes in the writing and extrusion speeds. Still, there are limitations such as the overall maximum velocity of the process, related to the mechanical transmission, and the movement precision or induced vibration.

The variety of materials previously referred to for FGF is available in the industry, directly obtained from chemical synthesis (virgin plastics of several grades) and recycling plants. In fact, the usage of recycled polymers in 3D printing has been investigated in or-der to reduce the environmental impact associated with "post-petroleum plastic sources" (16). Following this trend, this type of manufacture constitutes a possible promotor of the circular economy. This becomes effective by reintegrating the most widely used polymers in the first phases of the plastic value chain described by (23).

1.2 LDPE in 3D Printing

One of the most ubiquitous plastics is low-density polyethylene (LDPE). This polyolefin is mainly present in packaging, pipes, and houseware items, and is part of the seven main groups of recycled plastics (16,24). The use of LDPE in direct digital manufacturing is still very limited and challenging due to issues such as poor adhesion and high shrinkage (25,26). In fact, the production of LDPE filaments has been studied, tuning the extrusion parameters in order to produce usable filaments (27).

Nonetheless, the low melting temperature (typically from 105°C to 110°C) and the availability of great quantities at a small cost, turn the possibility of exploring a vast source of recycled raw material into an opportunity, increasing the value of extrusion-based 3D printing and the material itself.

Currently, LDPE has been studied in AM as a matrix for composites with higher biodegradability or with reinforcement particles (25, 28) as a potential material for patch antenna substrates (29), and as an additive itself on a blend with high-density polyethylene (HDPE) to fit its properties to 3D printing (25,30). Clearly, there is a wide interest on the application of this material in

3D printing, especially in the context of the implementation of circular economies. It is possible to incorporate additives in low-density polyethylene in order to promote dimensional accuracy, improve mechanical behavior (26, 31), and allow new applications. The exploration of material reinforcement is very significant when including recycled LDPE in the value chain since it has the potential of diluting the effects of degradation (from contaminants and broken molecular chains) induced by the recycling procedures. These additives work as nucleation agents which promote faster nucleation and a higher level of crystallinity, typically resulting in a higher rigidity. In the case of the present work, our ultimate goal is to reinforce the material by mapping its own properties during 3D printing, as a consequence of actively changing the process parameters. This paper describes the first of many studies to achieve that objective.

1.3 Melt flow conditions and morphology

The properties of objects manufactured from plastics do not entirely depend on the ingenuity of the molecule maker, as the structure and morphology which develop during the manufacturing process have a relevant role. In other words, the material properties are highly dependent on the process parameters. The most heavily used plastics in industry are semicrystalline (as it is possible to observe in (32)), in other words, they contain both amorphous and crystalline material. The majority of the matter is formed by the arrangement of single crystals, such as metals, in which the material consists of a large number of separate crystalline regions with grain boundaries between them. Large single crystals of polymers are not observed apart from the case of polydiacetylene which can be prepared from single crystals of the monomer via topochemical polymerization (33).

Crystallization processes, whether in a melt or in a solution, involve the processes of untangling the chains and then straightening them to add to the crystal growth face, although the precise details remain unclear. In 1957, a number of researchers deduced that the polymer chains folded at the top and bottom surfaces of the crystals which take the form of thin platelets about 10nm in thickness but up to several micrometers in the lateral directions (34).

Further work revealed that the chain folded lamellar crystals could develop in the framework of a spherulite in which crystals grew out from a common point in a crystallo-graphic direction lying in the plane of the lamellae (35).

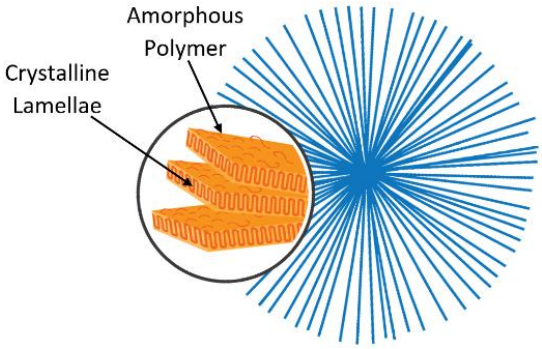

Figure 2 - Schematic representation of a spherulite (semicrystalline structure).

Spherulites have been widely studied in polymer science, and the relationships of spherulite morphology to mechanical and other properties have been extensively explored. For instance, it was shown in early studies that the number and size of spherulites are directly correlated with the yield point and overall physical behavior of polymers (36,37).

Some efforts to better understand the local mechanical properties have been deployed for mapping along the spherulite radius (38), and to manipulate these structures during the process, with

the application of new conditions such as nucleation agents and external loads, obtaining a better orientation of the lamellae and overall elongation (39).

Other arrangements are possible to observe when the lamellar crystals grow out from a common row nucleus, resulting in a higher level of anisotropy. Not surprisingly these different types of spatial arrangements exhibit different properties both with regard to mechanical behavior and degradation in the case of biodegradable polymers used in biomedical applications (40).

The formation of row nuclei can be associated with the development of extended chain conformations due to strain in a flow system (41). Equally highly anisotropic nanoparticles, such as carbon nanotubes (42) or self-assembling fibrillar nanoparticulate nucleating agents (43), can lead to higher anisotropic arrangements and a higher level of crystallinity. In the melt flow, this happens as a consequence of the common alignment of the nucleation sites, assuming that the common orientation of the particles introduced during the flow persists at the time crystallization is initiated.

The same mechanism can occur with the longest molecular chains in a polymer melt. this flow-induced orientation is often associated with the formation of shish-kebab semicrystalline structures (41,44) (represented in Figure 3).

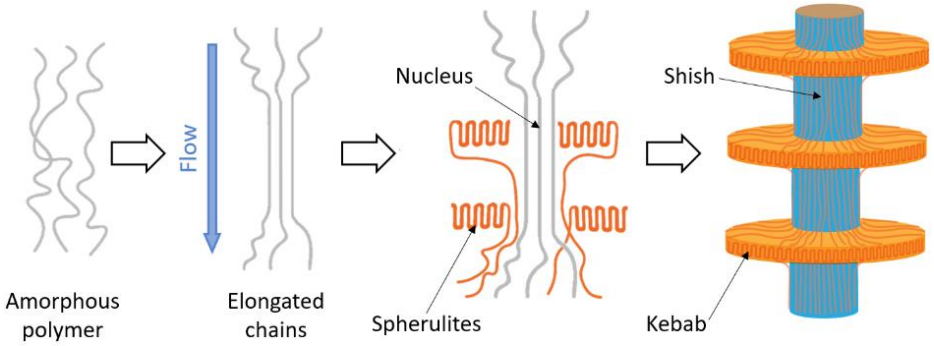

Figure 3 - Schematic representation of the formation of a shish kebab semicrystalline structure. Adapted from (45).

Basically, the longest chains (with higher molecular weight) become elongated due to the stresses in the flow. If, when reaching the crystallization temperature, these chains remain elongated, they template the nucleation (acting as row nuclei) for the surrounding polymer melt and chain folded lamellar crystals to grow out from. These lamellar crystals have their growth direction normal to the nuclei formed from the elongated chains (46).

In extrusion-based 3D printing, independently of the plastic part design, the polymer in the liquid phase is forced to pass through a restricting die (nozzle) with a certain length-to-diameter ratio (L/D). Even considering that the extrudate swells at the exit of the extruder (47), the resultant strand diameter is mainly defined by the nozzle diameter, and consequently, it defines the printing resolution, as observed in Figure 4.

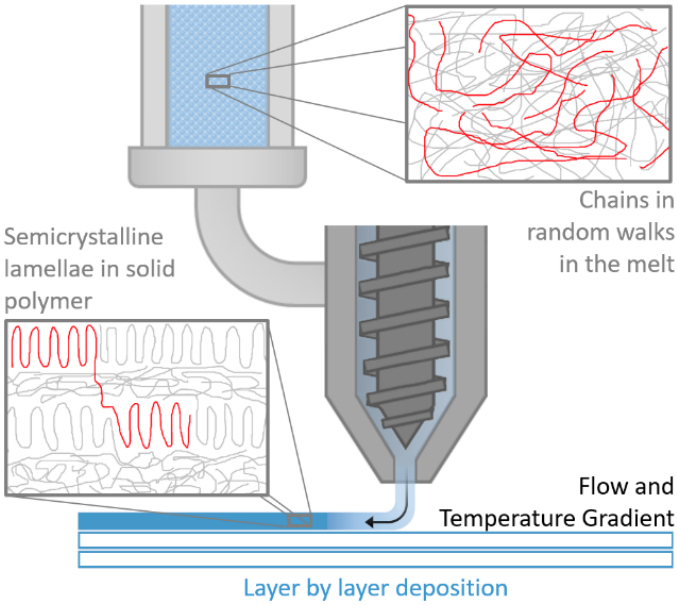

Figure 4 - Representation of the polymer morphology overall change during FGF 3D printing. The two highlights, from left to right, respectively correspond to the melt in the reservoir and the deposited extrudate along the print.

Shear stresses are applied in order to force the melt to pass through a constricted zone. For semicrystalline polymers (as it is illustrated in Figure 4), this condition induces the elongation of the larger chains (48), which can generate flow-induced oriented structures such as the shish-kebab arrangements presented in Figure 3. In practice, this results in a higher proportion of crystalline to amorphous material.

These higher levels of preferred molecular alignment are expected to be translated into having a significant impact on the mechanical properties of the manufactured part. As an example, 3D printed objects can be mapped to be much stiffer in the longitudinal axis of the extruded strands, contrasting with a typical isotropic structure regularly obtained.

2 Materials and Methods

2.1 Samples Material

In this experiment, the samples correspond to the in-situ produced extrudates of semicrystalline thermoplastic. With the 3D printer analogous equipment, the trials were performed with low-density polyethylene (LDPE) from Repsol, the Alcudia® 1970C, with a melt flow index of 7.5 g/10min.

2.2 X-ray Scattering Experimental Setup

For the realization of the morphology analysis, the X-ray scattering was performed with synchrotron radiation, similarly to what has been performed by Mitchell, et al. (49); utilizing an especially developed apparatus, in this case, to replicate the extrusion-based 3D printer operation at the beamline. The facilities and the equipment are followingly de-scribed in the subsections 2.2.1 and 2.2.2.

SAXS/WAXS Beamline

Small-angle X-ray scattering (SAXS) and wide-angle X-ray scattering (WAXS) measurements were performed at the ALBA Synchrotron Light Source in Barcelona, using the NCD-SWEET Beamline (50). This beamline has equipment for the capture of SAXS and WAXS patterns

simultaneously. The SAXS patterns were obtained in a Q-range from 0.002 $Å^{-1}$ to 0.125 $Å^{-1}$ and the WAXS patterns from 1.0 $Å^{-1}$ to 3 $Å^{-1}$. The SAXS Detector is a Pilatus3S 1M system from DECTRIS, a hybrid single photon counting system. The X-ray photon absorption in the detector leads to the formation of electron-hole pairs and a charge proportional to the photon energy.

The Pilatus system is constituted by an arranged set of silicon sensors, and as a con-sequence, approximately ~7% of the detector is intrinsically inactive (this unutilized zone appears as a black stripes grid in the intensity recordings. Regarding the charge, it is detected and processed by the pixel readout system, and the effective pixel has a dynamic range of 20 bits and a size of 172 x 172μm. In order to prevent the saturation of the detector, a beam stop is placed in front of the detector to absorb the zero-angle transmitted beam. The sample to SAXS detector distance was 6.73 m with an incident X-ray wave-length of 1 Å. The detector orientation and sample-to-detector distance were calibrated using the well-known standard silver behenate.

The WAXS detector was a Rayonix LX255 HS which is a triple cooled CCD detector bonded to fiber optic tapers to the X-ray photon detector surface, with a pixel size of 44.27x44.27 μm. The geometry of the detector ensures that the direct beam and the SAXS pattern are not blocked by itself. The WAXS orientation and sample to detector distance were calibrated using Cr2O3. For each 2D SAXS pattern an azimuthal section I(α) was obtained at constant |Q| and as a function of α, which is the angle between the extrusion axis (vertical to the beamline) the beamline and the scattering vector Q. The values of I(α) were necessary to evaluate the level of preferred orientation of the chain folded lamellar crystals (given by $<P_{2n}>_Q$), using the methodology developed by Mitchell (51–53), represented in the equation below.

$$< P_{2n} >_Q = \frac{1}{(4n+1)P_2{}^m} \int_0^{\pi/2} \frac{I\left(\left|\underline{Q}\right|, \alpha\right) \sin\ \alpha P_2\ (\cos\alpha)\ d\alpha}{I(\left|\underline{Q}\right|, \alpha) \sin\alpha\ d\alpha} \qquad \text{(Equation 1)}$$

This equation describes the orientation distribution function of the normal vectors to the lamellar crystals (Q). The first component $<P_{2n}>$ is defined as the orientation parameter, and it reveals, on a scale from 0 to 1 the level of anisotropy of the polymer morphology: if $<P_{2n}>=0$, then the morphology is isotropic; if $<P_{2n}>=1$, then the crystals share the same alignment.

Beamline 3D Printer

One of the challenges of performing 3D printing trials at the ALBA synchrotron NCD-SWEET beamline consisted of the process and equipment adaptation. For the experiment with low-density polyethylene extrusion, the team of the present work resorted to the apparatus described in (14). It consists of a device that can be mounted on the standard sample platform, and it was designed to allow a continuous and stable extrusion, aligning the extrudate sample with the X-ray beam. The model of the printer and the schematic of the experiment are presented in Figure 5.

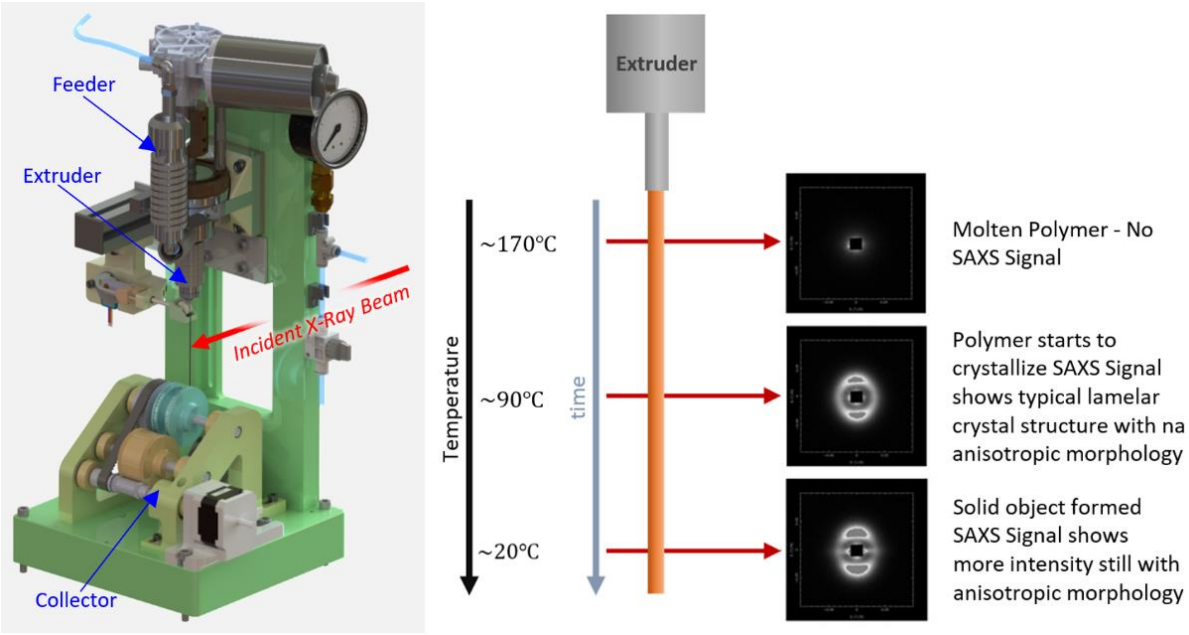

Figure 5 – (Left) A CAD representation of the 3D printer developed for this work. (Right) A schematic of the quasi-static state of the extrudate in a constant gradient of temperature (from the extrusion of the LDPE, passing through crystallization, until cooling down to the surrounding temperature). The evolution of structure can be evaluated by moving the incident X-ray beam down the jet. Adapted from (14).

Comprising three main parts (feeder, extruder, and rotating collector), this equipment simulates extrusion-based 3D printing along a moving platform, with a theoretically infinite path in a single deposition direction (for a wider testing window).

This system is adjustable in the cartesian axis and uses a single extruder with a dual channel screw to push the polymer melt through a needle with a high length-to-diameter ratio (L/D ≈36).

The FGF extruder utilized has a similar design to the one used in the bioextruder (20) (also developed by a team of CDRSP- Polytechnic of Leiria), and it corresponds to the con-figuration c) in Figure 1. Thus, it contains an attached material reservoir and three independent zones of temperature control.

The communication with a microcontroller board enables the remote operation of the apparatus, more specifically the control of the collector velocity (write/print speed), extruder screw rotation velocity (extrusion rate), and the nozzle wiping mechanism.

Below, in Figure 6, a representation of the experimental assembly is presented, showing the 3D printer mounted on the beamline platform, and the association of SAXS and WAXS detectors to the scales of observation: lamellae morphology (~100Å) and crystalline structures (~10Å), respectively.

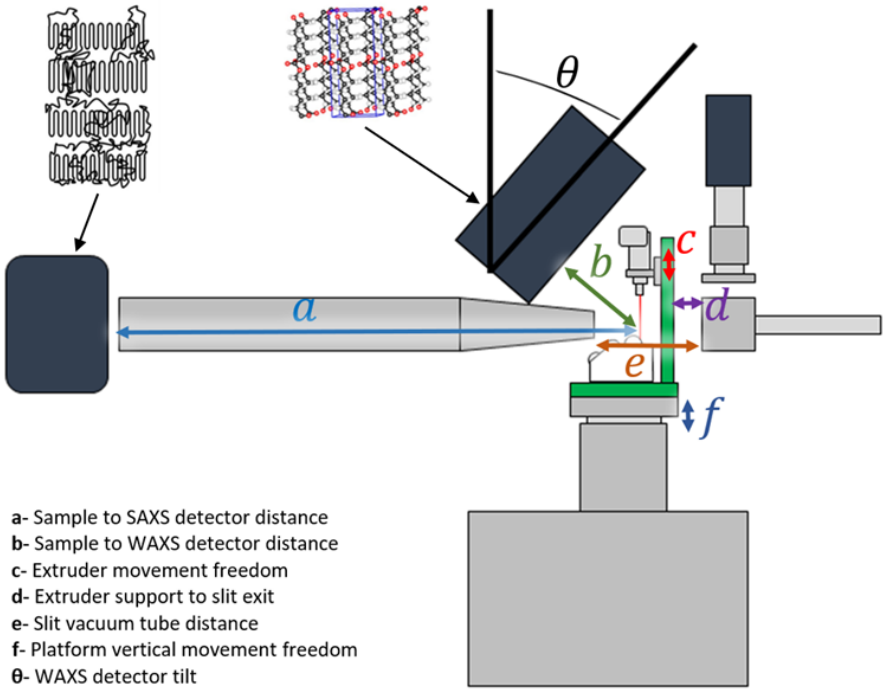

Figure 6 - Representation of the 3D printer analogous equipment mounted on the NCD-SWEET beamline at the ALBA Synchrotron Light Source, with the domain of pattern observation of each detector. Adapted from (14).

This representation shows the main dimensions related to the beamline facilities and the 3D printer. For the vertical adjustment of the area to be scanned, the distance between the needle outlet and the collector is variable by 50 mm.

The temperature profile of the extruded filament was maintained constant. Hence, it was possible to observe the extrudate in a quasi-steady state, in which the evolution of the structure and morphology with time could be assessed by moving up and down the platform; repositioning the incident X-ray beam along the extruded filament. Remotely and automatically controlled, a scan of 20 steps of 0.1mm with a 1-second data collection period could be retrieved, for each trial. A photograph of the equipment on the beamline is followingly presented in Figure 7.

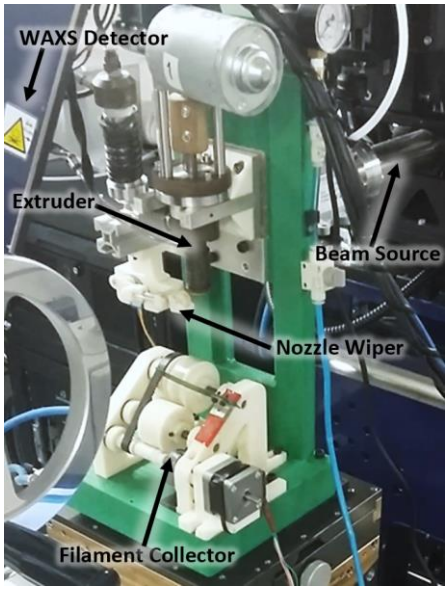

Figure 7 - Photograph of the equipment on the mounting stage of the beamline.

3 Results and Discussion

3.1 Crystallization Evaluation

The evaluation of the LDPE crystallization was performed using differential scanning calorimetry (DSC) with a with a PerkinElmer STA 6000 thermal analyzer. Samples were heated from 30°C to 150°C at a rate of 10°C/min. A steady state at the maximum temperature was maintained for 5 minutes, followed by cooling back to 30°C at a rate of 5°C/min. The final cooling stage is represented in Figure 8.

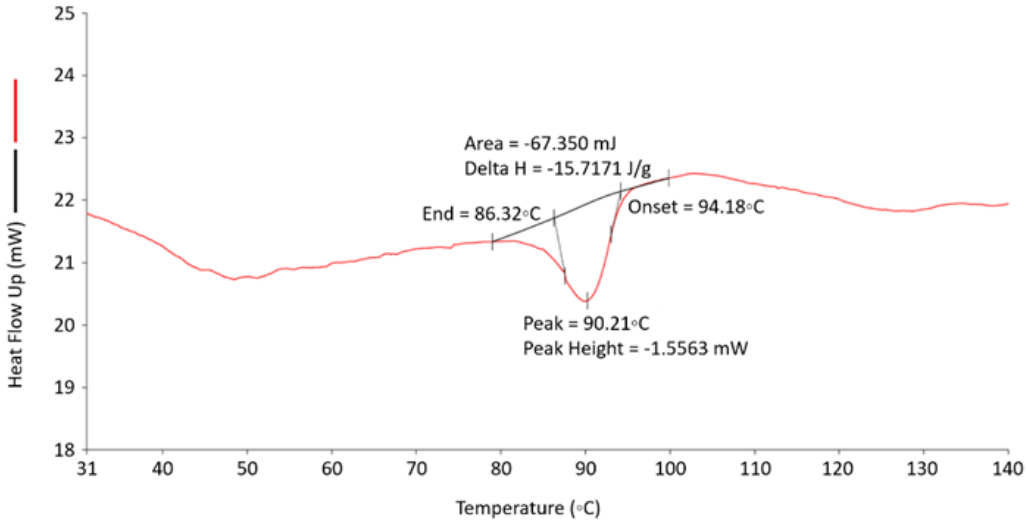

Figure 8 - DSC cooling scan of a sample of LDPE used in this work from 150°C to room temperature (around 30°C) showing the crystallization peak which reveals the maximum rate for a quiescent melt at 90.2°C.

In this domain of the DSC cooling scan, it is observed that in the quiescent material, the onset of crystallization occurs at 94.2 °C while the maximum rate of crystallization is observed to be at a

temperature of 90.2°C. Notice that the material which has been extruded may start to crystallize at a higher temperature than the observed with the quiescent material, due to the presence of flow-induced row nuclei.

3.2 X-ray Scattering Analysis

In this section, the results of the in-situ small and wide X-ray scattering analysis are presented. In Figure 9, the recorded SAXS scattering patterns of the filaments extruded with different write speeds (print speeds), maintaining the extrusion temperature and rate.

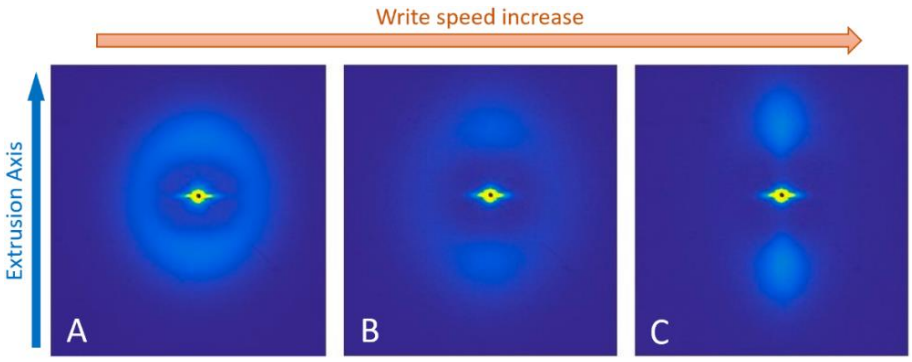

Figure 9 - SAXS patterns from the last point of each scan down the extruded filament, at a temperature of 170°C, and a constant extrusion rate with different write/print speeds (increasing from A to C). Adapted from (15).

These SAXS patterns correspond to the point just before the build platform and are typical for a semicrystalline polymer. Pattern A shows a practically isotropic ring, indicating an isotropic distribution of the lamellar crystals. On the other hand, Figure 9C exhibits a highly anisotropic distribution of scattering suggesting a higher degree of order of lamellar crystals. The middle pattern (B) corresponds to an intermediate write speed, and it comprises both isotropic and highly anisotropic scatterings.

The WAXS pattern presented in Figure 10 was recorded in the same instant as the Figure 9C SAXS pattern. It shows the intense peaks for LDPE, the 110 and 200, corresponding to the arcs observed from right to left. Moreover, the development of an anisotropic morphology is indicated by the variation of the peaks' intensity in the azimuthal range.

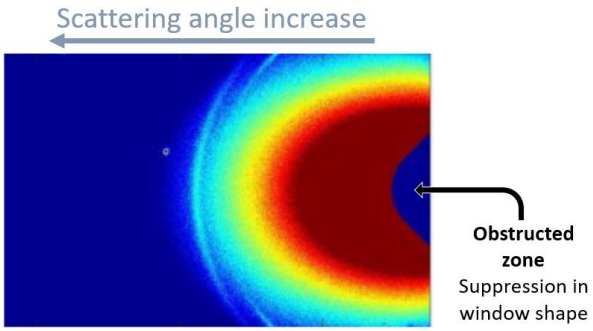

Figure 10 - WAXS pattern recorded at the same time as the SAXS pattern shown in Figure 9C. The scattering angle increases from left to right. Only the lower half of the angular range is shown in this figure, corresponding to a Q range of 1 to 2 $Å^{-1}$. Adapted from (15).

It is noticed that the anisotropy revealed in the WAXS pattern is less pronounced than the one observed with SAXS. This observation underlines the challenge of using wide-angle X-ray scattering to assess the orientation of structures in semicrystalline polymers. In the case of LDPE, the twisted

arrangement of chain-folded lamellar crystals is commonly observed. Thus, the preferred orientation of the lamellar crystals cannot be evaluated simply from WAXS patterns.

The preferred level of orientation of the lamellar crystals, the results are shown in Figure 11. The vertical axis corresponds to the orientation parameter $\langle P_{2n} \rangle$, obtained through Equation 1. Once again, this parameter can assume values from 0 to 1, respectively corresponding to a scale from completely isotropic to anisotropic morphology (uniform orientation of the crystalline structures).

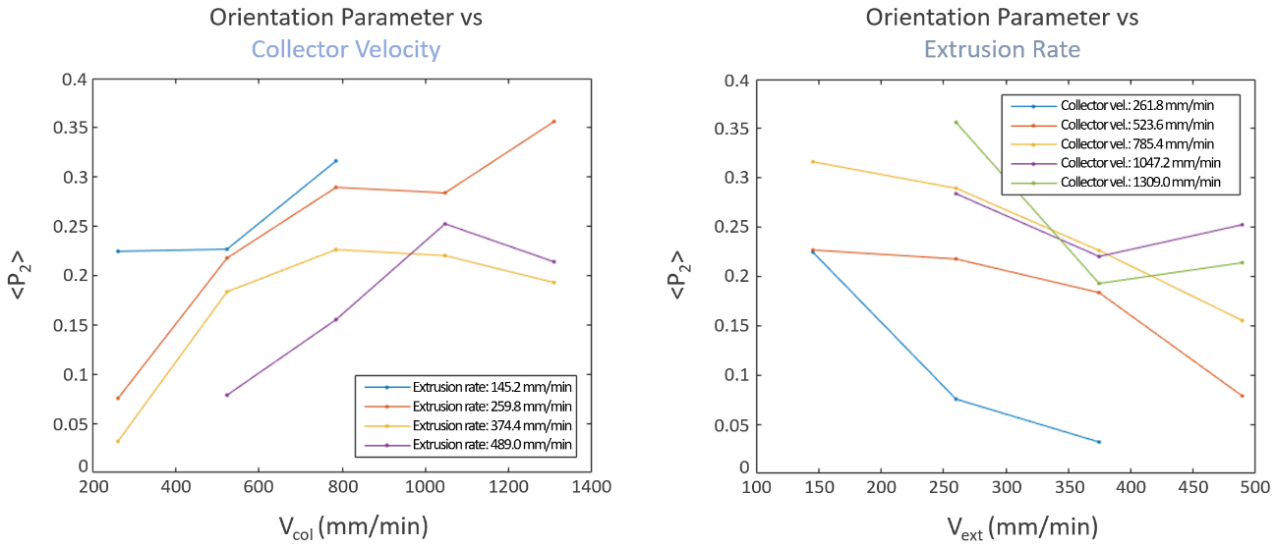

Figure 11 - Plots of the level of preferred orientation of the chain folded lamellar crystals in extruded strands of low-density polyethylene (LDPE) as a function of the collector velocity/print speed (on the left) and the extrusion velocity (on the right), at a constant extrusion temperature.

For the elaboration of both graphs, the temperatures of the 3 main zones of the extruder (feeder, channel, and extruder body) remained constant (extrusion temperature of 190°C). The left-hand plot corresponds to the variation of the preferred orientation level with the collector velocity (maintaining the extrusion rate value). The plot at the right corresponds to the variation of $\langle P_{2n} \rangle$ with the extrusion rate (at constant values of collector velocity). Notice that printing speed is represented by the collector main roll rotation velocity given by the product of its angular velocity and radius.

In order to display any correlations between the preferred molecular orientation and extrusion and collector velocities, the three-dimensional plot shown Figure 12 was prepared, with the combined data from both plots in Figure 11.

Clearly, from the obtained results, it is possible to observe the final anisotropy level in LDPE, establishing a briefer correlation with both the extrusion and writing/print speeds (this one represented by the collector velocity), with the help of a color scale. The dark blue corresponds to the isotropic zone, and the yellow zones correspond to the higher anisotropy levels.

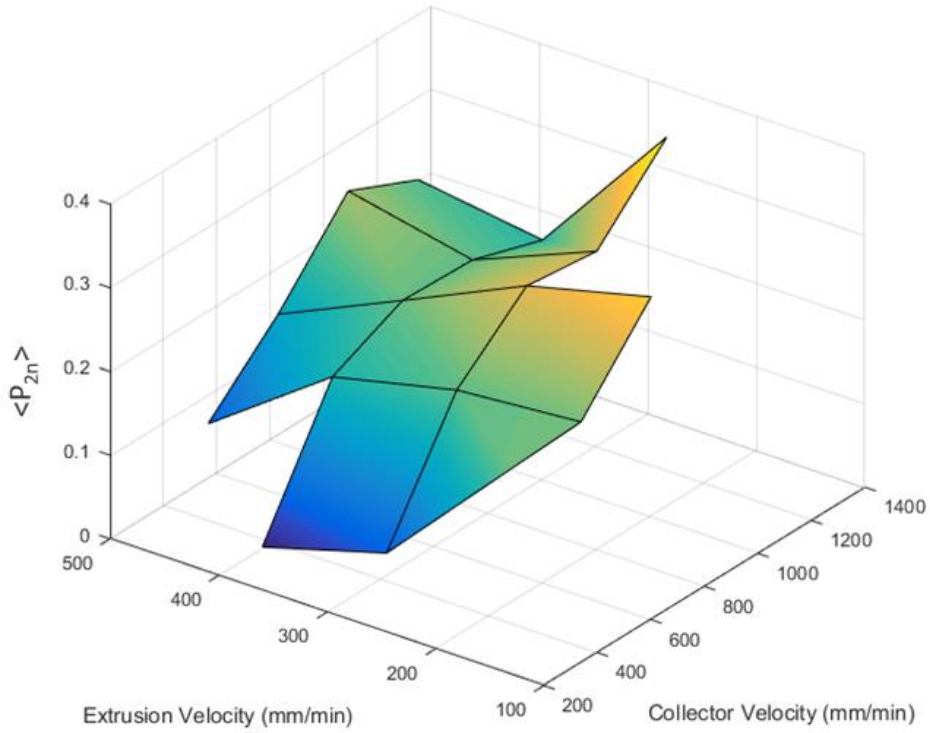

Figure 12 - Three-dimensional plot of the level of preferred orientation of the chain folded lamellar crystals in extruded strands of low-density polyethylene (LDPE) as a function of the extrusion velocity and the write speed (collector velocity) at a constant extrusion temperature, obtained from the conjunction of both graphs of Figure 11.

In summary, and in a broad observation, the level of preferred orientation of the chain folded lamellar crystals is directly proportional to the collector velocity (write/print speed) and inversely proportional to the extrusion rate.

In practice, during manufacturing, it represents that a more pronounced anisotropy value (associated with higher elastic modulus) (14) is reached while extruding a smaller amount of material along the same or a bigger path. This can be translated as a thinning of the deposited filament, and a faster cooling rate.

Particular attention has to be given to the faster cooling rates and the thinning of the extrudate, once it may compromise, in a counter-productive way, the interlayer adhesion, as well as the adhesion between subsequently deposited filaments. Consequently, it may affect the mechanical properties and behavior of the generated part (22).

This condition has to be considered in advance, during the part design. Usually, slicing software provides these correlations in order to accomplish the intended geometries. However, if the design for additive manufacturing strategy incorporates this thinning, another solution should be the revision of the number of cycles/scans to fulfill a given length/width. Given the circumstances, it is not clearly proven that faster deposition movements of the extrudate should consist of accelerated production. Therefore, we can-not conclude, at some other level of process optimization, and with the actual data, if the achievement of a higher level of anisotropy in semicrystalline polymers can be promptly or fully associated with more agile production cycles. The use of higher extrusion speed doesn't necessarily imply a higher manufacturing pace and may limit the overall rate of production.

Perhaps, new slicing strategies could be applied in order to optimize the anisotropy and, consequently, obtain well-defined stiffer and softer zones, while maintaining a relatively normal to fast-paced production.

4 Conclusions and Future Work

The main conclusion of the present work is that the adjustment of 3D printing parameters can be utilized strategically to affect the material morphology and structure along the fabrication of an object. Alternating the levels of preferred orientation of the lamellar crystals, it is possible to transcribe expected properties, correlated with the balance between isotropic and anisotropic distributions.

As an example, higher write speeds lead to faster cooling. For the same given temperature differential (from the nozzle to the cooled state of the deposited material), as the print speed increases, the extended chains, constrained and reoriented in the melt flow, don't have enough time to relax and remain mostly extended during crystallization, generating highly-aligned, therefore anisotropic morphology.

With a single material, the conception phase of a product can employ this morphology mapping strategy in order to set different mechanical properties. In the future, it should be expected the possibility to alter conditions and process parameters "on demand", during fabrication, to obtain desirable properties in particular zones of a single material manufactured part. This work is dedicated to promoting that approach, instead of considering, as in the current paradigm, that the pre-determined set of values should be maintained during the whole 3D printing production.

Certainly, and depending on the parameter to change (monitoring and control main variable), its set value is theoretically met within a certain period. How short or long that response turns out to be, in conjunction with the required time for those changes to have an effect on the material morphology, determines the resolution of the mapping.

Summarizing, controlling the core parameters of 3D printing induces changes in the material structure and morphology of semicrystalline polymers like LDPE. As a consequence, it is predicted that will affect the functionality of the printed part, allowing the enhancement of mechanical properties in a localized way. Therefore, more than reproducing a certain desired shape, it is believed that 3D printing may help develop new degrees of function for even more complex parts.

As this project is progressing, future works include studies about the rheological behavior, mechanical testing, 3D printing trials, the development of new products, and the influence of other variables such as the extrudate temperature.

5 Conflict of Interest

The funders had no role in the design of the study; in the collection, analyses, or interpretation of data; in the writing of the manuscript, or in the decision to publish the results.

6 Author Contributions

Conceptualization, GRM, DPS, JP; methodology, DPS. CKL, JCM, ES, GRM; software, GRM, JP.; validation, GRM, JP.; for-mal analysis, JP; investigation, JP, DPS, SA, PPF.; resources, X.X.; data curation, X.X.; writing—original draft preparation, DPS, GRM.; writing—DPS, JP, GRM PPF, X.X.; visualization, JP GRM.; supervision, GRM AM, PFF; project administration, GRM PPF; funding acquisition, GRM, PPF, AM. All authors have read and agreed to the published version of the manuscript.

7 Funding

This work is supported by the Fundação para a Ciência e Tecnologia (FCT) through the Project references: MIT-EXPL/TDI/0044/2021. It is also supported by the National Agency for Innovation (ANI) through the projects: UID/Multi/04044/2013; PAMI-Roteiro/0328/2013 (Nº 022158), Add.Additive - Add additive manufacturing to Portuguese industry PO-CI-01-0247-FEDER-024533 and UC4EP PTDC/CTM-POL/7133/2014).

8 Acknowledgments

These experiments were performed at NCD-SWEET beamline at ALBA Synchrotron with the collaboration of ALBA staff. We thank Miguel Belbut from CDRSP-IPLeiria for his help with the evaluation of the orientation parameter.

9 References

(1) Chen, D.; Heyer, S.; Ibbotson, S.; Salonitis, K.; Steingrímsson, J.G.; Thiede. S. Direct Digital Manufacturing: Definition, Evolution, and Sustainability Implications. J Clean Prod 2015, 107, 615–625. doi:10.1016/j.jclepro.2015.05.009.

(2) Paritala, P.K.; Manchikatla, S.; Yarlagadda, P.K.D. Digital Manufacturing- Applications Past, Current, and Future Trends. Procedia Eng 2017, 174, 982–991. doi:https://doi.org/10.1016/j.proeng.2017.01.250.

(3) Gibson, Ian, Rosen, David, Brent, S. Additive Manufacturing Technologies, 3D Printing, Rapid Prototyping, and Direct Digital Manufacturing.. 2015. ISBN 978-1-4939-2113-3.

(4) Morouço, P.; Biscaia, S.; Moura, C.; Alves, N.M. Biomedical Applications from a Direct Digital Manufacturing Perspective. Material Science and Engineering with Advanced Research. 2015. 15–17. doi:10.24218/msear.2015.13.

(5) Turner, B.N.; Gold, S.A. A Review of Melt Extrusion Additive Manufacturing Processes: II. Materials, Dimensional Accuracy, and Surface Roughness. Rapid Prototyp J 2015. 21, 250–261, doi:10.1108/RPJ-02-2013-0017.

(6) Kristiawan, R.B.; Imaduddin, F.; Ariawan, D.; Ubaidillah; Arifin, Z. A Review on the Fused Deposition Modeling (FDM) 3D Printing: Filament Processing, Materials, and Printing Parameters. 2021, 11, 639–649. doi:doi:10.1515/eng-2021-0063.

(7) Duan, M.; Yoon, D.; Okwudire, C.E. A Limited-Preview Filtered B-Spline Approach to Tracking Control – With Application to Vibration-Induced Error Compensation of a 3D Printer. Mechatronics 2018. 56, 287–296, doi:https://doi.org/10.1016/j.mechatronics.2017.09.002.

(8) Durakovic, B. Design for Additive Manufacturing: Benefits, Trends and Challenges. Periodicals of Engineering and Natural Sciences 2018, 6, 179–191, doi:10.21533/pen.v6i2.224.

(9) Fico, D.; Rizzo, D.; Casciaro, R.; Corcione, C.E. A Review of Polymer-Based Materials for Fused Filament Fabrication (FFF): Focus on Sustainability and Recycled Materials. Polymers (Basel) 2022, 14, 1–35, doi:10.3390/polym14030465.

(10) Woern, A.L.; Byard, D.J.; Oakley, R.B.; Fiedler, M.J.; Snabes, S.L.; Pearce, J.M. Fused Particle Fabrication 3-D Printing: Recycled Materials' Optimization and Mechanical Properties. Materials 2018, 11, doi:10.3390/ma11081413.

(11) Nogales, A.; Gutiérrez-Fernández, E.; García-Gutiérrez, M.-C.; Ezquerra, T.A.; Rebollar, E.; Šics, I.; Malfois, M.; Gaidukovs, S.; Gēcis, E.; Celms, K.; et al. Structure Development in Polymers during Fused Filament Fabrication (FFF): An in Situ Small- and Wide-Angle X-Ray Scattering Study Using Synchrotron Radiation. Macromolecules 2019, 52, 9715–9723, doi:10.1021/acs.macromol.9b01620.

(12) Ezquerra, T.A.; Nogales, A.; García-Gutiérrez, M.C.; Rebollar, E.; Gálvez, O.; Šics, I.; Malfois, M. Probing Structure Development in Poly(Vinylidene Fluoride) during "Operando" 3-D Printing by Small and Wide Angle X-Ray Scattering. Polymer (Guildf) 2022, 249, doi:https://doi.org/10.1016/j.polymer.2022.124827.

(13) Shmueli, Y.; Jiang, J.; Zhou, Y.; Xue, Y.; Chang, C.-C.; Yuan, G.; Satija, S.K.; Lee, S.; Nam, C.-Y.; Kim, T.; et al. Simultaneous in Situ X-Ray Scattering and Infrared Imaging of Polymer Extrusion in Additive Manufacturing. ACS Appl Polym Mater 2019, 1, 1559–1567, doi:10.1021/acsapm.9b00328.

(14) da Silva, D.P.; Pinheiro, J.; Abdulghani, S.; Lorger, C.K.; Martinez, J.C.; Solano, E.; Mateus, A.; Pascoal-Faria, P.; Mitchell, G.R. Changing the Paradigm-Controlling Polymer Morphology during 3D Printing Defines Properties. MDPI Polymers 2022, 14, 1–14, doi:10.3390/polym14091638.

(15) Silva, D.; Abdulghani, S.; Kamma-lorger, C.S.; Solano, E.; Martinez, J.C.; Pascoal-faria, P.; Mateus, A.; Mitchell, G.R. Controlling Morphological Development during Additive Manufacturing : A Route to the Mapping of Properties †. 2022, 3–7.

(16) Mikula, K.; Skrzypczak, D.; Izydorczyk, G.; Warchoł, J.; Moustakas, K.; Chojnacka, K.; Witek-Krowiak, A. 3D Printing Filament as a Second Life of Waste Plastics—a Review. Environmental Science and Pollution Research 2021, 28, 12321–12333, doi:10.1007/s11356-020-10657-8.

(17) Cruz Sanchez, F.A.; Boudaoud, H.; Hoppe, S.; Camargo, M. Polymer Recycling in an Open-Source Additive Manufacturing Context: Mechanical Issues. Addit Manuf 2017, 17, 87–105, doi:10.1016/j.addma.2017.05.013.

(18) Shaik, Y.P.; Schuster, J.; Shaik, A. A Scientific Review on Various Pellet Extruders Used in 3D Printing FDM Processes. OAlib 2021, 08, 1–19, doi:10.4236/oalib.1107698.

(19) Whyman, S.; Arif, K.M.; Potgieter, J. Design and Development of an Extrusion System for 3D Printing Biopolymer Pellets. International Journal of Advanced Manufacturing Technology 2018, 96, 3417–3428, doi:10.1007/s00170-018-1843-y.

(20) Almeida HA, Bártolo PJ, Mota CM, M.A. 2010 Processo e Equipamento de Fabrico Rápido Por Bioextrusão 2010.

(21) Volpato, N.; Kretschek, D.; Foggiatto, J.A.; Gomez da Silva Cruz, C.M. Experimental Analysis of an Extrusion System for Additive Manufacturing Based on Polymer Pellets. International Journal of Advanced Manufacturing Technology 2015, 81, 1519–1531, doi:10.1007/s00170-015-7300-2.

(22) Geng, P.; Zhao, J.; Wu, W.; Ye, W.; Wang, Y.; Wang, S.; Zhang, S. Effects of Extrusion on Speed and Printing Speed on the 3D Printing Stability of Extruded PEEK Filament. J Manuf Process 2019, 37, 266–273, doi:10.1016/j.jmapro.2018.11.023.

(23) Johansen, M.R.; Christensen, T.B.; Ramos, T.M.; Syberg, K. A Review of the Plastic Value Chain from a Circular Economy Perspective. J Environ Manage 2022, 302, 113975, doi:10.1016/j.jenvman.2021.113975.

(24) Achilias, D.S.; Roupakias, C.; Megalokonomos, P.; Lappas, A.A.; Antonakou, V. Chemical Recycling of Plastic Wastes Made from Polyethylene (LDPE and HDPE) and Polypropylene (PP). J Hazard Mater 2007, 149, 536–542, doi:10.1016/j.jhazmat.2007.06.076.

(25) Verma, N.; Awasthi, P.; Gupta, A.; Banerjee, S.S. Fused Deposition Modeling of Polyolefins: Challenges and Opportunities. Macromol Mater Eng 2023, 308, doi:https://doi.org/10.1002/mame.202200421.

(26) Olesik, P.; Godzierz, M.; Kozioł, M. Preliminary Characterization of Novel LDPE-Based Wear-Resistant Composite Suitable for FDM 3D Printing. Materials 2019, 12, doi:10.3390/ma12162520.

(27) Stanciu, N.; Stan, F.; Fetecau, C.; Serban, A. Fabrication and Characterization of LDPE and HDPE Filaments for 3D Printing. Journal of Engineering Sciences and Innovation 2018, 3, 299–312.

(28) Pantyukhov, P.; Kolesnikova, N.; Popov, A. Preparation, Structure, and Properties of Biocomposites Based on Low-Density Polyethylene and Lignocellulosic Fillers. Polym Compos 2016, 37, 1461–1472, doi:10.1002/pc.23315.

(29) Singh, R.; Kumar, S.; Singh, A.P.; Wei, Y. On Comparison of Recycled LDPE and LDPE–Bakelite Composite Based 3D Printed Patch Antenna. Proceedings of the Institution of Mechanical Engineers, Part L: Journal of Materials: Design and Applications 2022, 236, 842–856, doi:10.1177/14644207211060465.

(30) Chatkunakasem, P.; Luangjuntawong, P.; Pongwisuthiruchte, A.; Aumnate, C.; Potiyaraj, P. Tuning of HDPE Properties for 3D Printing. Key Eng Mater 2018, 773 KEM, 67–71, doi:10.4028/www.scientific.net/KEM.773.67.

(31) Bedi, P.; Singh, R.; Ahuja, I.P.S. Effect of SiC/Al2O3 Particle Size Reinforcement in Recycled LDPE Matrix on Mechanical Properties of FDM Feed Stock Filament. Virtual Phys Prototyp 2018, 13, 246–254, doi:10.1080/17452759.2018.1496605.

(32) Geyer, R.; Jambeck, J.R.; Law, K.L. Production, Use, and Fate of All Plastics Ever Made. Sci Adv 2017, 3, 3–8, doi:10.1126/sciadv.1700782.

(33) Enkelmann, V. Structural Aspects of the Topochemical Polymerization of Diacetylenes. 1984, 91–136, doi:10.1007/bfb0017652.

(34) Keller, A. A Note on Single Crystals in Polymers: Evidence for a Folded Chain Configuration. The Philosophical Magazine: A Journal of Theoretical Experimental and Applied Physics 1957, 2, 1171–1175, doi:10.1080/14786435708242746.

(35) Bassett, D.C. Lamellar Organization in Polymer Spherulites. In Integration of Fundamental Polymer Science and Technology; Kleintjens, L.A., Lemstra, P.J., Eds.; Springer Netherlands: Dordrecht, 1986; pp. 466–470 ISBN 978-94-009-4185-4.

(36) Starkweather, H.W.; Brooks, R.E. Effect of Spherulites on the Mechanical Properties of Nylon 66. J Appl Polym Sci 1959, 1, 236–239, doi:10.1002/app.1959.070010214.

(37) Pavlov, V.I. Investigation of the Effect of Spherulite Size on the Strength and Deformation Characteristics of Isotactic Polypropylene Films. Soviet Materials Science 1971, 4, 438–440, doi:10.1007/BF00721450.

(38) Enrique-Jimenez, P.; Vega, J.F.; Martínez-Salazar, J.; Ania, F.; Flores, A. Mapping the Mechanical Properties of Poly(3-Hydroxybutyrate-Co-3-Hydroxyvalerate) Banded Spherulites by Nanoindentation. MDPI Polymers 2016, 8, doi:10.3390/polym8100358.

(39) Huan, Q.; Zhu, S.; Ma, Y.; Zhang, J.; Zhang, S.; Feng, X.; Han, K.; Yu, M. Markedly Improving Mechanical Properties for Isotactic Polypropylene with Large-Size Spherulites by Pressure-Induced Flow Processing. Polymer (Guildf) 2013, 54, 1177–1183, doi:10.1016/j.polymer.2012.12.055.

(40) Shah, T. v.; Vasava, D. v. A Glimpse of Biodegradable Polymers and Biomedical Applications. E-Polymers 2019, 19, 385–410, doi:10.1515/epoly-2019-0041.

(41) P J Phillips Polymer Crystals. Reports on Progress in Physics 1990, 53, 549, doi:10.1088/0034-4885/53/5/002.

(42) Li, L.; Li, B.; Hood, M.A.; Li, C.Y. Carbon Nanotube Induced Polymer Crystallization: The Formation of Nanohybrid Shish-Kebabs. Polymer (Guildf) 2009, 50, 953–965, doi:10.1016/j.polymer.2008.12.031.

(43) Shazleen, S.S.; Yasim-Anuar, T.A.T.; Ibrahim, N.A.; Hassan, M.A.; Ariffin, H. Functionality of Cellulose Nanofiber as Bio-Based Nucleating Agent and Nano-Reinforcement Material to Enhance Crystallization and Mechanical Properties of Polylactic Acid Nanocomposite. MDPI Polymers 2021, 13, 1–19, doi:10.3390/polym13030389.

(44) Keller, A. Long-Chain Polymer Crystals. Phys Today 1970, 23, 42–50, doi:10.1063/1.3022109.

(45) Dargazany, R.; Khiêm, V.N.; Poshtan, E.A.; Itskov, M. Constitutive Modeling of Strain-Induced Crystallization in Filled Rubbers. Phys Rev E Stat Nonlin Soft Matter Phys 2014, 89, doi:10.1103/PhysRevE.89.022604.

(46) Somani, R.H.; Yang, L.; Zhu, L.; Hsiao, B.S. Flow-Induced Shish-Kebab Precursor Structures in Entangled Polymer Melts. Polymer (Guildf) 2005, 46, 8587–8623, doi:10.1016/j.polymer.2005.06.034.

(47) Wang, K. Die Swell of Complex Polymeric Systems. In Viscoelasticity - From Theory to Biological Applications; de Vicente, J., Ed.; IntechOpen, 2012; pp. 77–96 ISBN 978-953-51-0841-2.

(48) Rubinstein, M., Colby, R. Polymer Physics; Oxford University Press, 2003; ISBN 019852059X.

(49) Pople, J.A., Mitchell, G.R., Chai, C.K. In-Situ Time-Resolving Wide-Angle X-Ray Scattering Study of Crystallization from Sheared Polyethylene Melts. Polymer (Guildf) 1996, 4187–4191, doi:10.1016/0032-3861(96)00264-9.

(50) González, J.B., González, N., Colldelram, C., Ribó, L., Fontserè, A., Jover -Manas, G., Villanueva, J., Llonch, J., Peña, G., Gevorgyan, A., Nikitin, G., Martínez, J.C., Kamma-Lorger, C., Solano, E., Sics, I., Ferrer, S., M.M. NCD-SWEET Beamline Upgrade. In Proceedings of the MEDSI2018 Proceedings of the 10th Mechanical Engineering Design of Synchrotron Radiation Equipment and Instrumentation Paris; Paris. France.

(51) Lovell, R., and Mitchell, G.R. Molecular Orientation Distribution Derived from an Arbitrary Reflection. Acta Crystallographica Section A 1981, 135–137.

(52) Mitchell, G.R.; Saengsuwan, S.; Bualek-Limcharoen, S. Evaluation of Preferred Orientation in Multi-Component Polymer Systems Using x-Ray Scattering Procedures. Prog Colloid Polym Sci 2005, 130, 149–158, doi:10.1007/b107341.

(53) Mohan, S.D., Olley R.H., Vaughan, A.S., Mitchell, G.R. Controlling the Morphology of Polymers: Multiple Scales of Structure and Processing.; Mitchell, G.R., Tojeira, A. Springer, 2016; ISBN 978-3-319-39320-9.

10 Data Availability Statement

The data obtained using the facilities of the ALBA Synchrotron Light Source are subject to the Generic data management policy at ALBA CELLS as can be accessed at Microsoft Word - Data_policy_Alba_v1.2_2017.doc (cells.es). The experimental data identifiers are available from the corresponding author after the end of the embargo period.